Chapter 3
Estimates of Wave Breaking Energy Dissipation Rate from Measurements of Whitecap Coverage

Adrian H. Callaghan

Abstract The easiest way to identify the occurrence, or recent occurrence of oceanic air-entraining breaking waves (whitecaps) from above the water surface is through photographic remote sensing of the sea surface. In this paper I estimate the energy dissipation rate due to breaking wave whitecaps using measurements of whitecap coverage of the sea surface. Several datasets are used that employed different methodologies for determining the whitecap coverage spanning almost 4 decades of research. The results show that, on average, the ratio of the energy dissipation rate due to whitecaps to the wind energy input rate to the upper ocean and wave field is close to unity above wind speeds of about 10 m s^{-1}. Below 10 m s^{-1}, this energy flux ratio decreases steadily from unity as wind speed decreases, in agreement with several recent studies. The implication is that other dissipative processes play an important role in dissipating the wind energy input to the upper ocean and wave field at low wind speeds. These results suggest that variability in this energy flux ratio may be responsible for differences in measurements and parameterisations of whitecap coverage at low wind speeds.

3.1 Introduction

"Anyone who has stood on a clifftop and looked seaward on a windy day is aware that whitecaps are brighter than those regions of the sea surface which are devoid of bubble rafts" (Monahan and O'Muircheartaigh 1986). The essence of this statement has influenced much of the remote sensing of sea surface whitecaps for almost half a century (Monahan 1971), and continues to be the basis on which new datasets of breaking wave whitecaps are collected and analysed with routine digital image acquisition and automated analysis procedures (Brumer et al. 2017). The associated broadband scattering of light by the turbulent aerated two-phase flow allows whitecaps to be recorded, measured and analysed in terms of areal coverage of the sea surface, whitecap kinematics and energy dissipation (Melville and Matusov 2002;

A. H. Callaghan (✉)
Department of Civil and Environmental Engineering, Imperial College London, London, UK
e-mail: a.callaghan@imperial.ac.uk

P. Vlahos (ed.), *Recent Advances in the Study of Oceanic Whitecaps*,
https://doi.org/10.1007/978-3-030-36371-0_3

Monahan and O'Muircheartaigh 1980; Schwendeman et al. 2014). Therefore, it is precisely because of their nature that whitecaps are an important driver of air-sea exchange processes and that whitecap occurrence can be measured with conventional photographic remote sensing techniques.

Whitecap foam at the ocean surface indicates the occurrence or recent occurrence of air-entraining wave breaking. The turbulent two-phase flow associated with whitecaps plays a critical role in many bubble-mediated air sea fluxes. Consequently, many studies have sought to characterise the relationships between air-sea fluxes of heat, gas and mass with the instantaneous coverage of the sea surface in whitecap foam, termed whitecap coverage (W). For example, E.C. Monahan and colleagues have used measurements and parameterisations of whitecap coverage to estimate variability in air-sea exchange of gas, sea spray aerosols, heat and carbon, as well as looking at effects of whitecaps on ocean acoustics (Andreas and Monahan 2000; Monahan and Spillane 1984; Monahan et al. 1982, 1986; Monahan and Lu 1990; Monahan and Dam 2001; Monahan and Callaghan 2015).

It is clear that much work has been carried out to relate the whitecap coverage of the oceans to various air-sea exchange processes. Moreover, an improved physical understanding and interpretation of whitecap coverage has the potential to benefit parameterisations of a wide number of air-sea exchange and upper ocean properties. Whitecap coverage is critically related to the rate of energy dissipation by whitecaps (S_{wcap}), such that if S_{wcap} is known, it should be possible to estimate W. Conversely, if W is measured, then estimates of S_{wcap} could be made. A quantitative relationship between S_{wcap} and W can introduce new possibilities to estimate W on a global scale using spectral wave models, thus moving away from single parameter wind speed parameterisations of W. This is desirable because sea state, wave breaking and whitecap-driven energy dissipation are not uniquely controlled by wind speed. In recognition of the importance of sea state in driving variability in whitecap coverage, several recent studies have parameterised and modelled whitecap coverage in terms of wind and sea state variables (Anguelova and Hwang 2016; Brumer et al. 2017; Scanlon et al. 2016).

In this paper, I follow the model outlined in Callaghan (2018) and derive estimates of S_{wcap} using measurements of whitecap coverage from several field datasets that also contain estimates of the wave energy dissipation rate, S_{ds}. The model emphasises the 3-dimensional nature of whitecaps with an explicit representation of the bubble plume penetration depth beneath actively breaking whitecaps. The model also accounts for the fraction of the wind energy input that is not dissipated by whitecaps, but by other processes. In a stationary sea state that is in dynamical equilibrium with the overlying wind forcing, the rate wind energy input to the wave field and upper ocean (S_{in}) is balanced by the wave field energy dissipation rate, and it is expected that $S_{in} \approx S_{ds}$. Several distinct physical processes contribute to S_{ds} such as Langmuir turbulence, micro-breaking waves, swell wave dissipation and whitecapping. Therefore, inverse estimates of S_{wcap} from observations of whitecap coverage can be a useful tool to evaluate the dissipative role of whitecapping in comparison to the other dissipative processes listed above. Recent work by Sutherland and Melville (2015), and subsequently by Banner and Morison (2018), suggest

that in old, swell dominated seas at low wind speeds, the energy flux ratio S_{wcap}/S_{in} can be as low as 0.1–0.2. Constraining variability in S_{wcap}/S_{in}, therefore has important implications for how whitecap coverage, and bubble-mediated air sea exchange processes, might be parameterised in terms of wind speed or S_{in}.

The paper proceeds as follows. Section 3.2 presents an overview of the Callaghan (2018) model. Estimates of S_{wcap} are made in Sect. 3.3 and compared to values of S_{in} and the variability in S_{wcap}/S_{in} is explored as a function of wind speed. This is followed by some conclusions in Sect. 3.4.

3.2 The Whitecap Energy Dissipation Model

The model relating the energy dissipation rate of whitecaps to whitecap coverage is described in Callaghan (2018) (hereafter referred to as C18), and a brief overview is given here. The model is derived from the laboratory results of Callaghan et al. (2016) which relates the total energy dissipated by a single breaking wave to the volume of the two-phase flow integrated in time until the maximum whitecap foam area is reached. This quantity is called the volume-time-integral (VTI). The breaking waves used in Callaghan et al. (2016) (hereafter referred to as CDS16) were unforced 2-dimensional breaking waves generated in a wave channel at the Scripps Institution of Oceanography. The experiments showed a linear relationship between the VTI and the measured total energy dissipation (ΔE_T – kg m^2 s^{-2}) for a series of 20 breaking wave packets that varied from weakly spilling to strongly plunging. Specifically, the following relationship was found:

$$\Delta E_T = \Omega \rho A_o \widehat{z}_p \tau_{growth} \tag{3.1}$$

Here, ρ is water density, A_o is the maximum foam area of a whitecap during wave breaking, $\widehat{z}_p$ is the whitecap area-weighted average bubble plume penetration depth during active wave breaking (see CDS16 for further details), and τ_{growth} is an integral timescale that characterises the breaking wave duration. Together, the terms $A_o \widehat{z}_p \tau_{growth}$ quantify the VTI of an individual breaking wave. The term Ω is the turbulence strength parameter with units W kg^{-1}. Its value was found to be 0.88 ($\pm$0.04) W kg^{-1}, determined as the slope of a least mean-squares linear fit between the measured ΔE_T and the VTI. This model was also found to be an excellent fit to the combined laboratory datasets of Duncan (1981), Lamarre and Melville (1991), and Blenkinsopp and Chaplin (2007).

Taking Eq. (3.1) as a representative model of the energy dissipated by a single whitecap, C18 derived a relationship between the energy dissipation rate of a population of whitecaps (S_{wcap}, with units W m^{-2}), whitecap coverage and the ensemble average bubble plume penetration depth of the total whitecap population ($\widehat{z}_p^*$). The model can be written in terms of total whitecap coverage (W) or growth phase whitecap coverage (W_{growth}). The latter determines the contribution of

whitecap foam area from actively breaking waves only, thereby neglecting the foam coverage contribution from decaying whitecap foam patches W_{decay} which is driven by degassing bubble plumes and surfactant effects (Callaghan et al. 2017). The whitecap energy dissipation rate models using W_{growth} and W are written, respectively, as:

$$S_{wcap} = \Omega \rho \widehat{z}_p^* W_{growth} = S_{in} - S_{other} \tag{3.2}$$

and

$$S_{wcap} = \frac{\Omega \rho \widehat{z}_p^* W}{(1+\delta)} = S_{in} - S_{other} \tag{3.3}$$

The right hand side of Eqs. 3.2 and 3.3 recognises the fact that energy dissipation by whitecaps is not the only process responsible for energy dissipation. The term S_{in} quantifies the rate of energy input to the wave field and upper ocean from the overlying wind field, and S_{other} quantifies the energy dissipation by processes such as the mechanical wind stirring of the upper-ocean, Langmuir turbulence and swell wave dissipation. The δ term in Eq. 3.3 is defined as the ratio of decay phase whitecap coverage to growth phase whitecap coverage, W_{decay}/W_{growth}, and the analysis of oceanic whitecaps in CDS18 suggest that its value is an increasing function of $\widehat{z}_p^*$.

There are some important points to mention about Eqs. 3.2 and 3.3. Firstly, Eq. 3.2 suggests that both W_{growth} and $\widehat{z}_p^*$ are needed to estimate S_{wcap} because a value of W_{growth} may not necessarily have a unique value of $\widehat{z}_p^*$. This relationship stems directly from the results of CDS16 which shows that VTI during the whitecap growth phase is linearly proportional to the total energy dissipated by the breaking wave. Therefore, the whitecap energy dissipation rate for a population of whitecaps is inextricably linked to both the surface whitecap coverage and the average vertical bubble plume penetration depth.

Secondly, it is only when S_{other} is negligible that S_{wcap} can be assumed to be approximately equal to S_{in}. This has shown to be true in ocean measurements of Sutherland and Melville (2015). The implications of this will be explored in more detail in Sect. 3.3.

Finally, whitecap coverage can be written as the sum of the whitecap coverage growth and decay contributions such that $W = W_{growth} + W_{decay}$. The decay term can be further decomposed into a degassing term, W_{degas} and a surfactant stabilised term, W_{stab}. The degassing term (W_{degas}) recognises the fact that after active breaking has ceased, the optically resolvable surface whitecap is only sustained for as long as there is a sufficient flux of bubbles to the water surface (Callaghan et al. 2013; Monahan and O'Muircheartaigh 1986). Therefore, the value of W_{degas} is directly dependent on $\widehat{z}_p^*$ because deeper bubble plumes take longer to rise to the surface.

Once at the surface, whitecap foam can be stabilised by naturally occurring surfactants that act to reduce the rate at which fluid drains from the whitecap foam

cell walls thereby extending the lifetime of patches of whitecap foam. The consequence is that W can also be affected by variations in water chemistry or surfactant concentration and type. Little is known about the magnitude of this surfactant effect, but previous studies suggest that the contribution of foam streaks to W, caused by surfactant-driven foam stabilisation, becomes larger with increasing wind speed, especially at wind speeds above 15 m s^{-1} (e.g. Holthuijsen et al. 2012; Ross and Cardone 1974). Callaghan et al. (2017) defined a foam stabilisation metric, Θ, to quantify surfactant-driven foam stabilisation of individual whitecaps and found that Θ tended to increase with increasing wind speed, in general agreement with Ross and Cardone (1974) and Holthuijsen et al. (2012).

The previous analysis indicates that using W in place of W_{growth}, but without accounting for how W is influenced by surfactant stabilisation effects would lead to an overestimation of S_{wcap}. When W_{stab} is negligible, however, the δ term in Eq. 3.3 can be parameterised in terms of $\widehat{z}_p^*$ alone, and either W or W_{growth} can be used to estimate S_{Wcap} as described in C18. In the analysis that follows, it is assumed that $W_{stab} \approx 0$ such that $W_{degas} = W_{decay}$.

In order to use either Eqs. 3.2 or 3.3 to estimate S_{wcap}, an estimate of $\widehat{z}_p^*$ is required. A wind speed dependent parameterisation of $\widehat{z}_p^*$, was proposed by C18, and is given by:

$$\widehat{z}_p^* = 0.0098 \frac{u_{10}^2}{g} + 0.02 \tag{3.4}$$

The parameterisation was derived from field observations of the ratio of stage A whitecap coverage (W_A) to whitecap coverage reported in Scanlon and Ward (2016). In C18, the assumption that $W_{growth} \approx W_A$ was made which allowed the measured ratio W_A/W to be used to estimate the value of $\widehat{z}_p^*$ as a function of u_{10} following the model in C18. Stage A whitecap coverage has been defined by Monahan and Woolf (1989) as the "surface manifestation of plunging aerated plumes" and it is directly linked to actively breaking whitecaps. W_{growth} is a measure of the foam area integrated in time from incipient breaking to maximum foam area and is therefore also related to the active phase of wave breaking. Therefore, the assumption that $W_{growth} \approx W_A$ is reasonable.

3.3 Results and Discussion

In this section the whitecap model described in Sect. 3.2 is applied to two datasets of whitecap coverage measurements and used to estimate S_{wcap}. These datasets also have accompanying estimates of the wave field energy dissipation rate, S_{ds}. In what follows the assumption of dynamical equilibrium is applied such that $S_{in} \approx S_{ds}$, thereby characterising a stationary wave field in dynamical equilibrium with the overlying wind forcing. This assumption neglects energy attributed to wave growth,

and is expected to be accurate within 5–10% (Hwang and Sletten 2008). The assumption of $S_{in} \approx S_{ds}$ was also made in C18, however in that study, independent estimates of S_{ds} were not used, and were determined from the overlying wind speed. Therefore, the present datasets to be used have more direct estimates of S_{ds} than C18.

The two datasets of measurements used in this study are taken from Hwang and Sletten (2008) (hereafter referred to as HS08) and Hanson and Phillips (1999) (hereafter referred to as HP99), and details of these are given below. These datasets are used to estimate the energy dissipation rate due to whitecaps, S_{wcap}, and the ratio S_{wcap}/S_{in} as a function of wind speed. The use of a wide range of datasets of whitecap coverage from various authors is useful because of the disparity of measurement and image analysis techniques used.

3.3.1 The TLS and HP99 Datasets

HS08 collected a dataset of whitecap coverage, wind speed and wave field measurements from the studies of E C Monahan (1971), Toba and Chaen (1973), Ross and Cardone (1974), Xu et al. (2000), (Lafon et al. 2004, 2007), and Sugihara et al. (2007), which was collectively termed "MTRXLS" in HS08. Of these datasets, Toba and Chaen (1973), Lafon et al. (2004, 2007) and Sugihara et al. (2007) were accompanied by wave measurements. Data from these studies will be used in this study, and the collective dataset is termed "TLS" hereafter. The wave measurements consisted of values of wave peak frequency (ω_p) and significant wave height (H_S), and the whitecap measurements were of total whitecap coverage, W. The wave energy dissipation rate (S_{ds}) estimates were calculated in HS08 as $S_{ds} = \alpha \rho_{air} U_{10}^3$, where $\alpha = 0.20\omega_*^{3.3}\eta_*$. The terms ω_* and η_* are non-dimensional wave frequency and non-dimensional wave variance, respectively, as defined in HS08 to which the reader is referred. These data were kindly provided by P. Hwang.

HP99 made measurements of the wave spectrum in the North Pacific and used accompanying measurements of Stage A whitecap coverage, W_A, which were provided by E.C. Monahan from the Monahan and Wilson (1993) study. The in-situ measured wave spectrum data were used to calculate S_{ds} following the equilibrium range theory of Phillips (1985). The HP99 dataset is characterised by variable wind forcing and mixed wave conditions which were often swell-dominated (see their figures 1 and 2). Furthermore, their S_{ds} calculations showed strong correlation with wind acceleration: for a given wind speed, S_{ds} was larger in decreasing winds than in rising winds. The HP99 data used here were digitised from their Figure 10 and Figure 11.

Figure 3.1a shows the wind speed dependence of the TLS W dataset and the HP99 W_A dataset. As expected, the HP99 W_A datapoints fall below the TLS W data. Both datasets exhibit scatter of 1–2 orders of magnitude at low wind speeds and this scatter tends to decrease with increasing wind speed. For example, the HP99 data show a distinct decrease in scatter at wind speeds above 10 m s^{-1}. For reference,

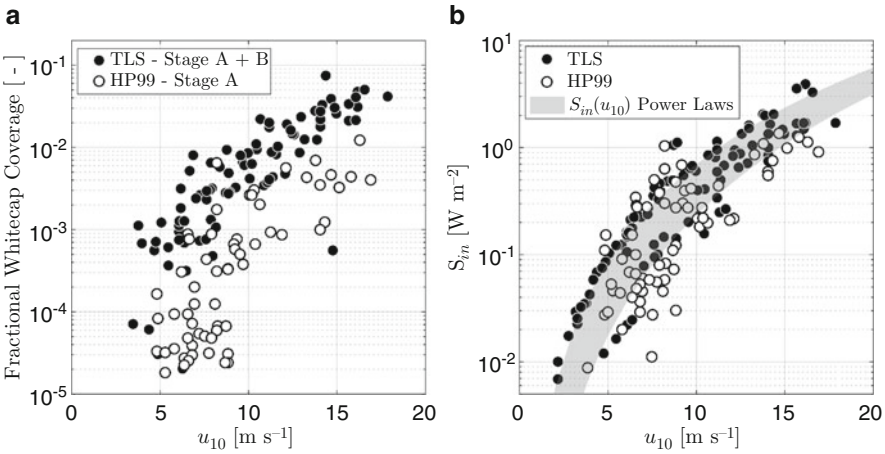

Fig. 3.1 (a, b). Panel (**a**) shows the variation of the measured whitecap coverage as a function of wind speed for the two datasets used here. The TLS dataset reports W measurements, whereas W_A was measured in HP99. Panel (**b**) shows the corresponding estimates of S_{in} derived from S_{ds} under the assumption that $S_{in} \approx S_{ds}$. The shaded region shows the range of $S_{in}(u_{10})$ estimates from the wind speed power laws reported in HP99, HS08 and C18

Figure 2 in HP99 shows that at wind speeds above about 10 m s^{-1}, the contribution of wind-wave significant wave height to the overall significant wave height increases signifying the decreasing contribution of swell waves to the overall wave spectral energy.

Figure 3.1b shows the estimates of the rate of energy input to the wave field and upper ocean (S_{in}) from each of the two datasets derived from wave field measurements under the assumption adopted here that $S_{in} \approx S_{ds}$. The shaded region shows the upper and lower range of S_{in} as a function of u_{10} from parameterisations reported in HS08 and HP99. The figure clearly demonstrates that while S_{in} is a strong function of wind speed, variations in sea state at a given wind speed introduce up to an order of magnitude variability in S_{in}.

3.3.2 *Variation in* $\mathbf{S_{wcap}}$ *as a Function of* $\mathbf{u_{10}}$

Estimates of S_{wcap} can be made for the TLS and HP99 datasets from their whitecap and wind speed measurements, along with the estimate of $\widehat{z}_p^*$ from Eq. 3.4. Note that for the HP99 dataset, the assumption that $W_{growth} \approx W_A$ has been made. Furthermore, for the TLS dataset, the assumption of negligible foam stabilisation by surfactants has been made, and equation (21) in C18 has been used to estimate δ in Eq. 3.3.

Figure 3.2 shows the relationship between wind speed and S_{wcap} for both datasets together. Above wind speed of about 10 m s^{-1}, there is good agreement between the S_{wcap} estimates for both datasets. This is encouraging for several reasons. Firstly, the whitecap measurements were made with different photographic techniques ranging

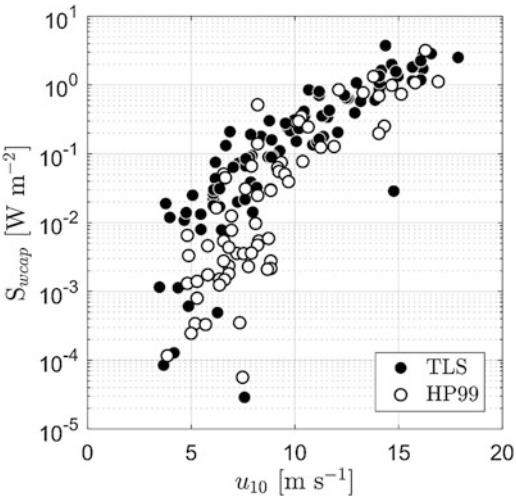

Fig. 3.2 The variation of the wave energy dissipation rate associated with whitecaps computed following the model in Callaghan (2018)

from the original manual analysis technique in Toba and Chaen (1973) to the digital image processing techniques in, for example, Sugihara et al. (2007). Secondly, the values of S_{wcap} were derived from both total whitecap fraction and growth phase whitecap fraction, measurements which often differ by a factor of 10 in magnitude as seen in Fig. 3.1a above. Thirdly, the S_{wcap} model was derived based upon unforced laboratory braking waves in a narrow wave channel, yet when applied to different whitecap datasets from different investigators provides good agreement in S_{wcap} at relatively high wind speeds.

At lower wind speeds below about 9–10 m s^{-1}, there is much more scatter in both datasets of S_{wcap}, and the HP99 values tend to lie below those of the TLS dataset. This may be explained by the very large swell presence in the wave field for the HP99 dataset, as evidenced by their figure 2. It has been shown in previous studies that in older-swell dominated seas, wave breaking is reduced and more variable compared to locally wind-driven seas (Callaghan et al. 2008b; Sugihara et al. 2007). Furthermore, the fraction of the wind energy input to the upper ocean that is dissipated by air-entraining whitecaps has been found to be reduced in low wind swell-dominated seas when compared to younger locally-forced wind-driven seas (Banner and Morison 2018; Sutherland and Melville 2013, 2015). This may be due to a misalignment of the wind stress and wind velocity vectors at low wind speeds caused by swell waves in a swell-dominated or mixed sea (Chen et al. 2018).

3.3.3 *Comparisons of* $\mathbf{S_{in}}$ *and* $\mathbf{S_{wcap}}$

In this section, the estimates of S_{wcap} generated for the TLS and HP99 datasets in Sect. 3.2 are compared against the corresponding estimates of S_{in}. This is done in

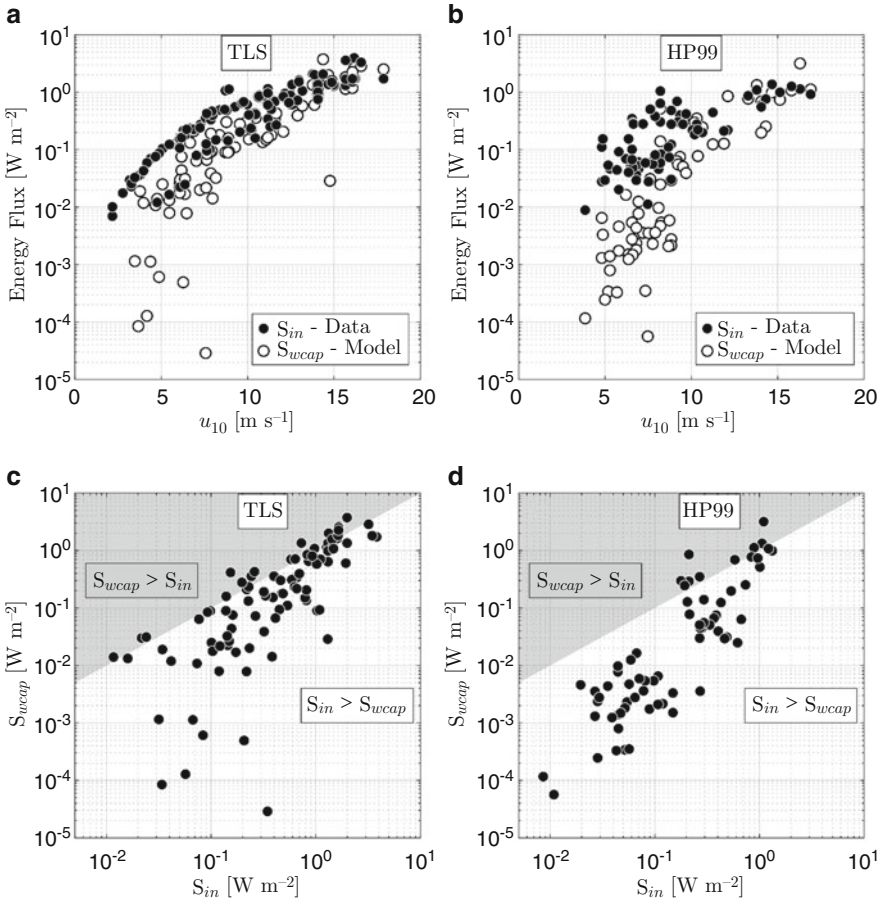

Fig. 3.3 **(a–d)** Panel a and panel b shows a comparison of the variation of S_{in} and S_{ds} as a function of wind speed for the TLS and HP99 datasets, respectively. Panel c and d are scatter plots of S_{in} and S_{ds} for the TLS and HP99 datasets, respectively. The grey shaded region is where the energy dissipation rate of whitecaps exceeds the energy input to the wave field from the overlying wind. Below the shaded region the energy input to the wave field from the overlying wind is greater than the energy dissipation rate of whitecaps

order to estimate how much of the wind energy input to the wave field is balanced by whitecap-driven energy dissipation.

Figure 3.3a, b show how S_{in} and S_{wcap} for the TLS and HP99 datasets vary with wind speed, respectively. In both datasets, there is a strong degree of overlap between the S_{in} and S_{wcap} values at wind speeds greater than about 9–10 m s^{-1}. The implication is that air-entraining whitecaps are the dominant mechanism of dissipating wave energy at these wind speeds, and they dissipate this energy in sufficient quantities to balance the energy input from the wind. This finding is in

general agreement with the field measurements of Sutherland and Melville (2015) and the conclusions of Banner and Morison (2018).

At lower wind speeds, the S_{wcap} model estimates tend to lie below the S_{in} measurements. The implication is that the relative importance of whitecapping as a dissipative mechanism reduces at low wind speeds and the relative dissipative role of other processes increases. Again, this agrees with the findings of Sutherland and Melville (2015) and Banner and Morison (2018). At these low wind speeds, the HP99 S_{wcap} estimates are consistently lower than S_{in}, which likely reflects the preponderance for reduced wave breaking in swell-dominated seas. For example, when Sugihara et al. (2007) classified their sea states as either pure wind-driven seas and seas with swell waves they found consistently lower whitecap coverage values in swell-dominated conditions than in pure wind seas (see their figure 12).

Figure 3.3c, d directly compare values of S_{wcap} and S_{in} for the TLS and HP99 datasets, respectively. In both datasets, it is clear that the estimated S_{wcap} rarely exceeds S_{in}. This result provides confidence that the C18 model provides realistic estimates of S_{wcap} from measurements of either W or W_{growth}. Importantly, it confirms the importance of incorporating a variable estimate of bubble plume penetration depth when interpreting whitecap measurements in terms of energy dissipation rate.

3.3.4 *Comparing of* S_{wcap}/S_{in} *to Field Data*

The results in Sect. 3.3.3 suggest that, at sufficiently large wind speeds, whitecaps are the dominant dissipative mechanism balancing the wind energy input to the wave field and upper ocean. To examine this more closely, the ratio S_{wcap}/S_{in} is plotted as a function of wind speed in Fig. 3.4a, b for the TLS and HP99 datasets, respectively. A value of unity suggests that wind energy input is balanced through dissipation by whitecaps.

At low wind speeds of less than about 10 m s^{-1}, there is a considerable degree of scatter in the S_{wcap}/S_{in} energy flux ratios, with many data points falling considerably below unity. This is a common feature in both datasets, but is more pronounced in the HP99 dataset, which may be a reflection of the strong swell influence at low wind speeds, as mentioned above. Indeed, the HP99 energy flux ratios do not approach unity until the wind speed exceeds 10 m s^{-1}. In contrast, the energy flux ratios in the TLS dataset do reach unity at wind speeds as low as 5 m s^{-1}, but also with considerable scatter.

At higher wind speeds of 10 m s^{-1} and above, most of the data points in figure 4a and figure 4b lie within a factor of 2 of unity. When the data points are averaged and binned by wind speed, the average data points lie very close to unity in the TLS dataset. There is somewhat more variability in S_{wcap}/S_{in} for the HP99 dataset, but still the variability is scattered around unity. Importantly in both datasets, there does not appear to any bias in S_{wcap}/S_{in} above or below unity at these larger wind speeds. The data suggest that on average, whitecapping is the dominant dissipative process at wind speeds above about 10 m s^{-1}, and is sufficient to balance the wind energy input.

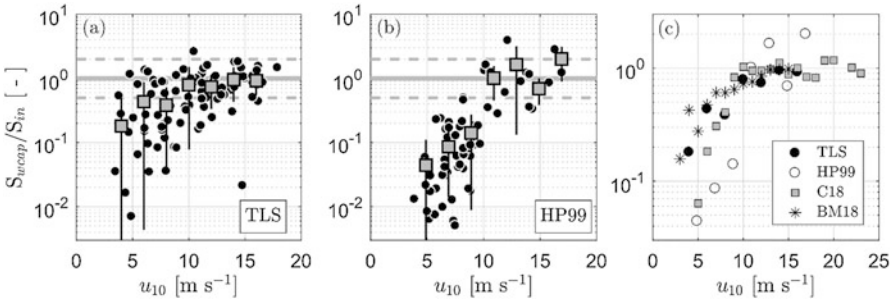

Fig. 3.4 **(a–c)** Panel a shows the ratio of the estimated energy dissipation rate due to whitecaps and wind energy input rate to the wave field for the TLS dataset. The squares are average values in 2 m s^{-1} wind speed bins, and vertical lines represent ±1 standard deviation around the mean. The solid grey line shows a value of unity, and the dashed lines show a variation of a factor of 2 around unity. Panel b has the same format as panel a but using the HP99 dataset. Panel c shows average values binned by wind speed for several datasets (note the change in vertical scale from panels a and b). The filled and open circles are the binned TLS and HP99 data from panel a and panel b, respectively. The grey squares are whitecap coverage based estimates from Callaghan (2018) (C18). The asterisks are derived from the *in-situ* ocean measurements of Sutherland and Melville (2015) as reported in Banner and Morison (2018) (BM18). Standard deviations of the mean data points have been omitted for clarity

In order to compare the energy flux ratio estimates from the TLS and HP99 datasets, Fig. 3.4c compares the bin average S_{wcap}/S_{in} values to average values from two other studies. Firstly, C18 use a dataset of whitecap coverage measurements to estimate S_{wcap} that span wind speeds of between 4 m s^{-1} and 23 m s^{-1} reported in Callaghan et al. (2008a). These data were taken as part of the Marine Aerosol Production (MAP) campaign which took place in the North Atlantic in the summer of 2006. Estimates of S_{in} for that study came from a least mean squares fit to the S_{wcap} data at wind speed above 10 m s^{-1}, which was then extrapolated to lower wind speeds. While this approach was a necessary approximation, these resulting estimates of $S_{in}(u_{10})$ were in excellent agreement with the $S_{in}(u_{10})$ parameterisations given in HS08 and HP99 for wind speeds larger than 10 m s^{-1}.

Secondly, but more importantly, data from figure 13 in BM18 were digitised and used to estimate S_{wcap} and S_{in}, and the ratio of these quantities is plotted as a function of wind speed plotted at 1 m s^{-1} intervals in Fig. 3.4c. These data originate from the field study of Sutherland and Melville (2015) from direct measurements of oceanic subsurface turbulence, the breaking wave field (including both micro-breakers and whitecaps) and the wind field.

The combined four S_{wcap}/S_{in} datasets, namely TLS, HP99, C18 and BM18, are plotted as a function of wind speed in figure 4c. Of these datasets, it is important to note that the BM18 is the most direct estimate. At wind speeds above 10 m s^{-1}, the average values of S_{wcap}/S_{in} fall very close to a value of unity, regardless of the origin of the dataset, albeit with the HP99 dataset showing larger fluctuations. This provides strong evidence supporting the data in Sutherland and Melville (2015) and the conclusions in Banner and Morison (2018), that at sufficiently large wind speeds

(i.e. $u_{10} \gtrsim 10$ m s^{-1}), when the wave field is less likely to be swell-dominated, whitecaps largely balance the wind energy input to the wave field and upper ocean. It is worth pointing out that the agreement between all four datasets at these wind speeds is excellent given that the S_{wcap} values of TLS, HP99 and C18 are derived from remote sensing of whitecaps from different studies, in different locations and using non-standardised image acquisition and analysis techniques.

The agreement in values of S_{wcap}/S_{in} at wind speeds greater than 10 m s^{-1}, mirrors the reduction in variability between whitecap coverage parameterisations where digital image analysis was used. As pointed out in Brumer et al. (2017) (see their Figure 1), there is much closer agreement between wind speed parameterisation of W above wind speeds of 10 m s^{-1} developed since 2007, when compared to datasets collected prior to this. This increase in agreement between wind speed parameterisations may reflect a move to more standardised image analysis techniques as suggested by Brumer et al. (2017). It may also be related to the larger image datasets that digital image analysis can enable, thereby decreasing uncertainty in whitecap coverage estimates at larger wind speeds where fewer data points have been collected.

As seen in Fig. 3.4c, agreement between the four datasets diminishes at lower wind speeds, accompanied by a decreasing trend in S_{wcap}/S_{in} values with decreasing wind speed. There is still a large degree of overlap between several of the studies, most notably BM18, TLS and C18, but the values of S_{wcap}/S_{in} from the different studies diverge as the wind speed drops. This is presumably a reflection of the different sea states between the studies at these low wind speeds. Indeed, at lower wind speeds, the presence of swell waves can have a much larger influence on the local wave field. Moreover, from *in-situ* measurements, Sutherland and Melville (2015) conclude that the dissipative contribution from whitecaps diminishes with increasing wave age characteristic of older swell-dominated seas.

Wind speed independent variability in wave age at low wind speeds is likely an important factor influencing wave breaking patterns which can drive large variability in values of S_{wcap}/S_{in}. One way in which variability in wave breaking patterns can be quantified at low wind speeds is by identifying the minimum wind speed at which whitecaps are first measured via photographic remote sensing of the ocean surface. This idea of a critical wind speed above which whitecaps can be recorded in images of the sea surface is encapsulated in terms of the Beaufort velocity (u_B) introduced by Monahan and O'Muircheartaigh (1986). As defined, the Beaufort velocity quantifies the wind speed at which there is a 50% chance of observing a whitecap in a set of images of the sea surface. Monahan and O'Muircheartaigh (1986) conclude that u_B is dependent on a range of factors, with water temperature and the stability of the lower atmosphere being of particular importance. For example, their Figure 2 suggests that u_B may extend from approximately 2 m s^{-1} to 7.5 m s^{-1} for a water-air temperature difference of +4 °C to −8 °C. In other words, whitecapping begins at lower wind speeds in conditions of unstable atmospheric stability. This view is supported qualitatively by Kraan et al. (1996) who commented that in their whitecap observations, there were "....two situations where no whitecaps were visible, though the wind speed was in the range 7-8 m s^{-1}". One of these instances occurred

in very stable atmospheric conditions, and the other in a neutrally stratified lower atmosphere. They also note that these observations occurred at times of strong tidal currents reaching magnitudes of 1 m s^{-1} which may have played a contributing role.

In addition to the Beaufort velocity set out in Monahan and O'Muircheartaigh (1986), previous studies have reported values of the critical wind speed above which whitecap coverage is non-zero. Estimates of this critical wind speed are found by fitting a model of the form $W = a(u_{10} - b)^n$ to a dataset of whitecap coverage and wind speed measurements. The value of the coefficient b represents the speed at which whitecapping is expected to begin. Values for this wind speed range between 2.56 m s^{-1} (Scanlon and Ward 2016) and to 6.33 m s^{-1} (Stramska and Petelski 2003) which are similar in magnitude to those reported in Monahan and O'Muircheartaigh (1986). The physical causes for the variation in this minimum critical wind speed are not entirely clear, but Stramska and Petelski (2003) suggest it is related to wave field development. Their data suggests that the onset of whitecapping is delayed in undeveloped or younger seas. In any case, it is evident from previous studies that a large degree of variability in wave breaking activity, and hence whitecap-driven energy dissipation can occur at wind speeds below about 8 m s^{-1}, in agreement with the data presented in Fig. 3.4 here.

3.4 Summary and Conclusions

The photographic observation of whitecaps at the ocean surface remains the most straightforward above-water method to detect the occurrence and scale of breaking waves in the ocean. The high reflectance of the aerated two-phase flow allows digital image remote sensing and subsequent image analysis techniques to return information on the properties of individual whitecaps, and populations of whitecaps, which can be used to estimate energy dissipation rates associated with breaking wave whitecaps.

This study has presented estimates of the energy dissipation rate of breaking wave whitecaps via the results of image analysis of sea surface images following the model presented in Callaghan (2018). The datasets used consisted of observations of both whitecap coverage and stage A, or growth phase, whitecap coverage, along with coincident measurements of wind and wave properties. To implement the model, the whitecap coverage measurements were combined with estimates of the average bubble plume penetration depth estimated from the wind speed parameterisation presented in Callaghan (2018). The wave measurements were used to calculate the dissipation rate of wave energy. The assumption of a stationary wave field was made such that total wave energy dissipation rate balanced the rate of wind energy input to the upper ocean and wave field. The estimates of the whitecap energy dissipation rate were then compared to coincident estimates of the wind energy input rate. This was used to determine the fraction of wind energy that is dissipated by whitecaps, and how this fraction varied as a function of wind speed.

These data were then compared to the results of Sutherland and Melville (2015), as presented by Banner and Morison (2018).

Under the constraints of the assumptions made here, as well as the assumptions inherent in the Callaghan (2018) model, the analysis in this study suggests that, on average in an equilibrium sea state, the fraction of the wind energy input to the wave field that is balanced by energy dissipation in whitecaps is not constant and typically increases with wind speed, approaching unity for wind speeds above 10 m s^{-1}. In other words, almost all of the wind energy input to the wave field is dissipated by whitecaps, with other dissipative processes playing a minor role at these wind speeds. This conclusion was found to be consistent across several different datasets, one of which was derived from direct oceanic turbulence and wave field measurements, with the others derived from remote sensing measurements of whitecaps and *in situ* wave field measurements. At lower wind speeds, below about 10 m s^{-1}, there is a large degree of variability in the energy flux ratio which ranged by up to two orders of magnitude from 1 to approximately 0.01for individual data points.

The results presented have implications for how either wind energy input models and energy dissipation rate in spectral wave models may be used to estimate air-sea bubble-mediated fluxes of gas and aerosol production, especially at low wind speeds. The analysis suggests, in line with the general conclusions of Sutherland and Melville (2015) and Banner and Morison (2018), that wave breaking whitecaps are not always the dominant mechanism balancing the wind energy input into the wave field at low wind speeds. It is speculated that variations in sea state at these low wind speeds, and in particular the presence or absence of swell, is responsible for this large variation. Further work is needed to constrain this variability in terms of wave field parameters. It should also be said that variability in how well wind energy input rate is estimated may also be important, but examining this in detail was beyond the scope of this study.

Finally, the estimates of the energy dissipation rate of whitecaps in this study provided an upper bound to the values of wind energy input. That provides further support that the model developed in Callaghan (2018), which was in part derived from a series of laboratory breaking wave experiments, is applicable to oceanic conditions. A key element of this model is the recognition that both the average bubble plume penetration depth and the surface whitecap coverage are needed to estimate the dissipation rate associated with whitecaps. Presently, the bubble plume penetration depth values used have been parameterised in terms of the wind speed raised to the power of 2. This functional form suggests that bubble plume penetration depth is proportional to the significant wave height of wind-forced waves, which has also been found to follow a similar wind speed dependence (Hanson and Phillips 1999). Further work is needed to develop a sea-state dependent parameterisation of bubble plume penetration depth, preferentially based on data from direct *in-situ* measurements.

Acknowledgements AHC gratefully acknowledges the provision of data from several studies by Paul Hwang. Funding for this study came from a Royal Society International Shooter Fellowship awarded to AHC. The author wishes to express his gratitude to E.C. Monahan for many helpful discussions on whitecaps.

References

Andreas, E. L., & Monahan, E. C. (2000). The role of whitecap bubbles in air–sea heat and moisture exchange. *Journal of Physical Oceanography, 30*(2), 433–442. https://doi.org/10.1175/1520-0485(2000)030<0433:Trowbi>2.0.Co;2.

Anguelova, M. D., & Hwang, P. A. (2016). Using energy dissipation rate to obtain active whitecap fraction. *Journal of Physical Oceanography, 46*(2), 461–481.

Banner, M. L., & Morison, R. P. (2018). On the upper ocean turbulent dissipation rate due to microscale breakers and small whitecaps. *Ocean Modelling, 126*, 63–76. https://doi.org/10.1016/j.ocemod.2018.04.004.

Blenkinsopp, C., & Chaplin, J. (2007). *Void fraction measurements in breaking waves*. Paper presented at proceedings of the Royal Society of London A: Mathematical, Physical and Engineering Sciences, The Royal Society.

Brumer, S. E., Zappa, C. J., Brooks, I. M., Tamura, H., Brown, S. M., Blomquist, B. W., Fairall, C. W., & Cifuentes-Lorenzen, A. (2017). Whitecap coverage dependence on wind and wave statistics as observed during SO GasEx and HiWinGS. *Journal of Physical Oceanography, 47*(9), 2211–2235. https://doi.org/10.1175/jpo-d-17-0005.1.

Callaghan, A. H. (2018). On the relationship between the energy dissipation rate of surface-breaking waves and oceanic whitecap coverage. *Journal of Physical Oceanography, 48*(11), 2609–2626. https://doi.org/10.1175/jpo-d-17-0124.1.

Callaghan, A., de Leeuw, G., Cohen, L., & O'Dowd, C. D. (2008a). Relationship of oceanic whitecap coverage to wind speed and wind history. *Geophysical Research Letters, 35*(23), n/a–n/a. https://doi.org/10.1029/2008GL036165.

Callaghan, A. H., Deane, G. B., & Stokes, M. D. (2008b). Observed physical and environmental causes of scatter in whitecap coverage values in a fetch-limited coastal zone. *Journal of Geophysical Research: Oceans, 113*(C5). https://doi.org/10.1029/2007JC004453.

Callaghan, A. H., Deane, G. B., & Stokes, M. D. (2013). Two regimes of laboratory whitecap foam decay: Bubble-plume controlled and surfactant stabilized. *Journal of Physical Oceanography, 43*(6), 1114–1126.

Callaghan, A. H., Deane, G. B., & Stokes, M. D. (2016). Laboratory air-entraining breaking waves: Imaging visible foam signatures to estimate energy dissipation. *Geophysical Research Letters, 43*(21), 11320–11328.

Callaghan, A. H., Deane, G. B., & Stokes, M. D. (2017). On the imprint of surfactant-driven stabilization of laboratory breaking wave foam with comparison to oceanic whitecaps. *Journal of Geophysical Research: Oceans, 122*(8), 6110–6128. https://doi.org/10.1002/2017JC012809.

Chen, S., Qiao, F., Huang, C. J., & Zhao, B. (2018). Deviation of wind stress from wind direction under low wind conditions. *Journal of Geophysical Research: Oceans, 0*(0). https://doi.org/10.1029/2018JC014137.

Duncan, J. (1981). *An experimental investigation of breaking waves produced by a towed hydrofoil*. Paper presented at proceedings of the Royal Society of London A: Mathematical, Physical and Engineering Sciences, The Royal Society.

Hanson, J. L., & Phillips, O. M. (1999). Wind sea growth and dissipation in the open ocean. *Journal of Physical Oceanography, 29*(8), 1633–1648.

Holthuijsen, L. H., Powell, M. D., & Pietrzak, J. D. (2012). Wind and waves in extreme hurricanes. *Journal of Geophysical Research: Oceans, 117*(C9), 1–15.

Hwang, P. A., & Sletten, M. A. (2008). Energy dissipation of wind-generated waves and whitecap coverage. *Journal of Geophysical Research: Oceans, 113*(C2), C02003.

Kraan, G., Oost, W., & Janssen, P. (1996). Wave energy dissipation by whitecaps. *Journal of Atmospheric and Oceanic Technology, 13*(1), 262–267.

Lafon, C., Piazzola, J., Forget, P., Le Calve, O., & Despiau, S. (2004). Analysis of the variations of the whitecap fraction as measured in a coastal zone. *Boundary-Layer Meteorology, 111*(2), 339–360.

Lafon, C., Piazzola, J., Forget, P., & Despiau, S. (2007). Whitecap coverage in coastal environment for steady and unsteady wave field conditions. *Journal of Marine Systems, 66*(1–4), 38–46.

Lamarre, E., & Melville, W. (1991). Air entrainment and dissipation in breaking waves. *Nature, 351*(6326), 469.

Melville, W. K., & Matusov, P. (2002). Distribution of breaking waves at the ocean surface. *Nature, 417*, 58. https://doi.org/10.1038/417058a.

Monahan, E. C. (1971). Oceanic whitecaps. *Journal of Physical Oceanography, 1*(2), 139–144.

Monahan, E. C., & Callaghan, A. H. (2015). *The discrete whitecap method for estimating sea salt aerosol generation: A reassessment*. Paper presented at 17th conference on atmospheric chemistry.

Monahan, E. C., & Dam, H. G. (2001). Bubbles: An estimate of their role in the global oceanic flux of carbon. *Journal of Geophysical Research: Oceans, 106*(C5), 9377–9383. https://doi.org/10.1029/2000JC000295.

Monahan, E. C., & Lu, M. (1990). Acoustically relevant bubble assemblages and their dependence on meteorological parameters. *IEEE Journal of Oceanic Engineering, 15*(4), 340–349.

Monahan, E. C., & O'Muircheartaigh, I. (1980). Optimal power-law description of oceanic whitecap coverage dependence on wind speed. *Journal of Physical Oceanography, 10*(12), 2094–2099. https://doi.org/10.1175/1520-0485(1980)010<2094:Opldoo>2.0.Co;2.

Monahan, E. C., & O'Muircheartaigh, I. G. (1986). Whitecaps and the passive remote sensing of the ocean surface. *International Journal of Remote Sensing, 7*(5), 627–642.

Monahan, E. C., & Spillane, M. C. (1984). The role of oceanic whitecaps in air-sea gas exchange. In W. Brutsaert & G. H. Jirka (Eds.), *Gas transfer at water surfaces* (pp. 495–503). Boston: Reidel.

Monahan, E. C., & Wilson, M. (1993). *Whitecap measurements. Critical Sea Test 7, Phase 2: Principal investigators' results*. The Johns Hopkins University Applied Physics Laboratory Tech. Rep. STD-R-2258, (808p, F. T. Erskine, & J. L. Hanson (Eds.)).

Monahan, E. C., & Woolf, D. K. (1989). Comments on variations of whitecap coverage with wind stress and water temperature. *Journal of Physical Oceanography, 19*(5), 706–709.

Monahan, E., Davidson, K., & Spiel, D. (1982). Whitecap aerosol productivity deduced from simulation tank measurements. *Journal of Geophysical Research: Oceans, 87*(C11), 8898–8904.

Monahan, E. C., Spiel, D. E., & Davidson, K. L. (1986). A model of marine aerosol generation via whitecaps and wave disruption. In *Oceanic whitecaps* (pp. 167–174). Dordrecht: Springer.

Phillips, O. (1985). Spectral and statistical properties of the equilibrium range in wind-generated gravity waves. *Journal of Fluid Mechanics, 156*, 505–531.

Ross, D. B., & Cardone, V. (1974). Observations of oceanic whitecaps and their relation to remote measurements of surface wind speed. *Journal of Geophysical Research, 79*(3), 444–452.

Scanlon, B., & Ward, B. (2016). The influence of environmental parameters on active and maturing oceanic whitecaps. *Journal of Geophysical Research: Oceans, 121*(5), 3325–3336. https://doi.org/10.1002/2015JC011230.

Scanlon, B., Breivik, Ø., Bidlot, J.-R., Janssen, P. A., Callaghan, A. H., & Ward, B. (2016). Modeling whitecap fraction with a wave model. *Journal of Physical Oceanography, 46*(3), 887–894.

Schwendeman, M., Thomson, J., & Gemmrich, J. R. (2014). Wave breaking dissipation in a young wind sea. *Journal of Physical Oceanography, 44*(1), 104–127. https://doi.org/10.1175/jpo-d-12-0237.1.

Stramska, M., & Petelski, T. (2003). Observations of oceanic whitecaps in the north polar waters of the Atlantic. *Journal of Geophysical Research: Oceans, 108*(C3), 3086.

Sugihara, Y., Tsumori, H., Ohga, T., Yoshioka, H., & Serizawa, S. (2007). Variation of whitecap coverage with wave-field conditions. *Journal of Marine Systems, 66*(1–4), 47–60.

Sutherland, P., & Melville, W. K. (2013). Field measurements and scaling of ocean surface wave-breaking statistics. *Geophysical Research Letters, 40*(12), 3074–3079.

Sutherland, P., & Melville, W. K. (2015). Field measurements of surface and near-surface turbulence in the presence of breaking waves. *Journal of Physical Oceanography, 45*(4), 943–965.

Toba, Y., and M. Chaen (1973), Quantitative expression of the breaking of wind waves on the sea surface, Rec. Oceanogr. Works Jpn., 12, 1–11

Xu, D., Liu, X., & Yu, D. (2000). Probability of wave breaking and whitecap coverage in a fetch-limited sea. *Journal of Geophysical Research: Oceans, 105*(C6), 14253–14259.